Ultra High Frequency-Low Intensity Magnetic Stimulation Enhances Functional Recovery in a Rat Model for Chronic Capsule Infarct

Zohaib Atif, Junsoo Kim, Ji-Young Park, Jongwook Cho, Suhyeon Kim, An Nazmus Sakib, Hyeon Seo, Chun Taek Lim, *Fellow IEEE*, Young Ro Kim, Euiheon Chung, Hyoung-Ihl Kim*, Hyuk-Sang Kwon*

***Abstract*—Stroke causes motor and cognitive impairments. Neural stimulation techniques such as repetitive transcranial magnetic stimulation (rTMS) and transcranial direct current stimulation (tDCS) has shown promise in rehabilitating impaired neural functions. However, despite the reported efficacies, stimulus parameters (i.e., applied field amplitude, frequency, and duration) are loosely defined and carry the risk of non-localized heat dissipation, seizure, and scalp discomfort due to high field intensities and direct contact of the devices with the scalp. To advance stroke therapy and to minimize their associated risks, we are exploring an alternative neuromodulation strategy termed ultra high frequency-low intensity magnetic stimulation (UHF-LiMS) designed to enhance functional recovery. For preclinical assessment, focal infarction was induced via photothrombosis in the internal capsule area of the subcortex in male Sprague-Dawley rats, a region well-documented for suppressing spontaneous longitudinal recovery. Sinusoidal magnetic fields (3–10 mT peak amplitude, 400 kHz) were applied, and functional recovery was assessed behaviorally and via imaging. In addition, longitudinal [^18F]-FDG microPET scans and immunohistochemical analysis of c-Fos expression were used to evaluate metabolic activity and neural activation at cellular level. Magnetic stimulation induced substantial somatomotor and somatosensory recovery, with behavioral scores improving by up to ~70% of pre-infarct levels. PET imaging showed reduced stroke-induced diaschisis and increased cortical and subcortical metabolic activity with statistically significant correlations. Elevated c-Fos expression in both cortical and subcortical regions indicates enhanced neuronal activation, serving as a transcriptional signature of neural plasticity. Our study demonstrates that UHF-LiMS effectively restores motor and sensory functions in a white matter stroke model, highlighting its therapeutic potential as a neurostimulation technique.**

***Index Terms*—UHF-LiMS, Ultra-high frequency low intensity magnetic stimulation, infarct capsule stroke, Longitudinal 2-deoxy-2-[18F]-fluoro-D-glucose microPET, metabolic activity, diaschisis, functional recovery.**

I. Introduction

Stroke is a leading cause of long-term disability, as it often leads to permanent deficits in sensory, language, and motor functions, thereby creating significant economic and emotional burdens where treatment options for chronic disease survivors remain limited [1-6]. Various neurorehabilitation methods have been developed to augment residual motor functions and to improve the quality of life [7] for stroke survivors [8-11]. In addition to brain stimulation techniques, stroke rehabilitation includes behavioral and task-oriented therapies such as constraint-induced movement therapy, technology-assisted approaches including robot-assisted rehabilitation, and

This work was supported by the National Research Foundation of Korea grant funded by the Korean Government Human Plus NRF-2019M3C1B8090841, and by Korean Government Ministry of Science and ICT under Grant No. NRF-2023R1A2C3002798, RS-2023-00264409, RS-2023-00302281, RS-2025-00522868, and RS-2025-00573499, and by the Brain Pool Program through the National Research Foundation of Korea (RS-2025-25418241). *(Corresponding author: Hyoung-Ihl Kim, PhD, MD, Hyuk-Sang Kwon, PhD).*

Zohaib Atif, J. Kim, J-Y. Park, S. Kim, A. N. Sakib, E. Chung, H-I. Kim, and MD H-S. Kwon* are with the Department of Biomedical Science and Engineering, Gwangju 61005, South Korea. (zohaibatif@gm.gist.ac.kr, jskim1098@gm.gist.ac.kr, mimi73@gist.ac.kr, suhyeonk@gm.gist.ac.kr, ansgalib@gm.gist.ac.kr, ogong50@gist.ac.kr, hyoungihl@gist.ac.kr, hyuksang@gist.ac.kr).

E. Chung, H-S. Kwon* are also with the AI Convergence School, and the Research Center for Photon Science Technology, Gwangju Institute of Science and Technology, Gwangju 61005, South Korea.

H. Seo, PhD is with the Department of Computer Science and Engineering Gyeongsang National University, Jinju, South Korea (hseo0612@gnu.ac.kr).

C. T. Lim, PhD is with the School of Electrical Engineering and computer Science, Gwangju Institute of Science and Technology, Gwangju 61005, South Korea (ctrim@gist.ac.kr).

Y. R. Kim, PhD is with the Athinoula A. Martinos Center for Biomedical Imaging, Massachusetts General Hospital, Charlestown, USA and the Department of Radiology; Harvard Medical School, Boston, MA, USA (yrkim@mgh.harvard.edu).

Jongwook Cho is with Biomedical Research Institute, Chonnam National University Hospital, Gwangju, 61469, South Korea (chojw@gm.gist.ac.kr)

peripheral neuromodulation strategies such as vagus nerve stimulation paired with rehabilitation training [12]. Among these methods, repetitive transcranial magnetic stimulation (rTMS) has been widely used to promote functional recovery in chronic stroke patients [6, 13, 14]. Current TMS protocols utilize high-intensity magnetic fields (1-2 Tesla) at the coil surface to induce cortical excitability changes typically within a frequency range of 1 to 100 Hz, with the aim of enhancing brain plasticity and function [15-17]. However, these high-intensity protocols pose safety concerns due to frequent exposure to strong magnetic fields, potentially increasing side effects such as seizures, syncope, headaches, local pain, and paresthesia [18, 19]. The International Commission on Non-Ionizing Radiation Protection (ICNIRP) and the U.S. National Institutes of Health (NIH) have established guidelines by defining safe exposure levels and distances [20]. Nevertheless, for the long-term safety of the patient population, exposure limits to non-ionizing radiation remains ill-defined and there is a need for alternative stimulation methods which minimize unnecessary risks in vulnerable patients. A recent report suggests that low-intensity, high-frequency magnetic stimulation could serve as a viable alternative. Labruna et al. have shown that kilohertz-frequency magnetic stimulation (2-3.5 kHz) can enhance cortical excitability [21]. Preclinical studies have shown that low-intensity magnetic stimulation (LiMS) induces adaptive changes in cortical neurons, characterized by enhanced synaptic plasticity, improved motor skill acquisition, increased expression of brain-derived neurotrophic factor (BDNF), and reduced action potential thresholds that facilitate greater neuronal excitability [22]. Moreover, LiMS applied at various frequencies and stimulation patterns regulate neuronal functions such as excitability [16, 23], plasticity [24], survival, and calcium signaling [25-27].

However, it has yet to be determined whether LiMS has any therapeutic efficacy as related to chronic stroke. A recent study demonstrated the biological effects of high-frequency magnetic pulses in the kHz to MHz range, particularly in the context of low-intensity magnetic stimulation, such as 1 MHz pulses, generates electric fields capable of penetrating neural tissue more efficiently while requiring less power compared to conventional TMS, thereby demonstrating the feasibility of integrating high-frequency, low-intensity stimulation, potentially opens new avenues for the therapeutic applications of TMS [18, 28]. Task-specific rehabilitation exercise (TSRE) is crucial for enhancing post-stroke recovery because it engages neural circuits underlying specific motor functions, particularly forelimb movement, thereby promoting targeted and functionally relevant neural plasticity [29], as approximately 30% of stroke survivors fail to regain full limb function and remain permanently disabled [30]. However, combining TMS with TSRE is challenging due to bulky TMS systems and the necessity for precise coil positioning over specific brain regions, further complicating mobility or wearable applications. Therefore, it became clear that these limitations need to be addressed to make the combination of TMS and TSRE a feasible treatment modality for treating chronic stroke and evaluating post-stroke outcome [31].

To address these challenges and to explore new therapeutic possibilities, we developed an innovative stimulation environment comprised of a controller, cooling system, power station, and a uniquely designed body coil capable of generating ultra high frequency-low intensity magnetic fields (UHF-LiMS). The coil's distinctive geometry ensures that an optimal magnetic field is distributed around the head, thereby facilitating awake stimulation in combination with task-specific exercises, such as the single pellet reaching task (SPRT). Our goal was to determine whether a novel stimulation protocol with task-specific exercises, in awake animals could promote functional recovery in a rat model for a severe chronic capsular stroke. Specifically, we investigated how UHF-LiMS contributes to post-stroke recovery, as evaluated by behavioral outcomes, longitudinal 2-deoxy-2-[18F]-fluoro-D-glucose microPET scans, and immunohistochemical analysis. Our study provides new insights into how the combination of high frequency-low intensity magnetic stimulation provides safer and more effective treatment modality for stroke rehabilitation.

II. Materials and Methods

A. Animals

All animal experimental procedures were approved by the Gwangju Institute of Science and Technology Animal Care and Use Committee (GIST-2019-074). Animal ARRIVE guidelines were followed in the preparation of the manuscript. This study used 32 male Sprague Dawley rats (9 weeks old, approximately 300 g), with eight animals assigned to each experimental group. The rats were housed in cages, with free access to both food and water at all times, and kept on a 12 h light/dark cycle (07:00–19:00) at 22℃ and 50% humidity.

B. Induction of Photothrombotic Capsular Infarction

Animals underwent photothrombotic stroke lesioning in the PLIC in the contralateral hemisphere of the preferred forelimb. Briefly, animals were anesthetized with a mixture of ketamine hydrochloride and xylazine and placed into a rodent stereotaxic frame. Rectal temperature was maintained at 37.5℃ using heating pad. After a scalp incision, a small hole was drilled and an optical fiber (core diameter of 62.5 μm and an outer diameter of 125 μm) was stereotaxically inserted into the PLIC (AP = -2.0 mm, ML = ±3.1 mm DV = 7.8 mm from the bregma). Rose Bengal dye (20 mg/kg) was then injected intravenously and the rats were irradiated for 1.5 minutes using a green laser (3.7 mW). After laser irradiation, the optical fiber was removed, the scalp wound sutured, and the animals were treated with ketoprofen (2 mg/kg, i.m.) for postoperative pain control.

C. Computational Modeling of the Electrical Field

Computational models were developed using images from a computerized tomography (CT) scan of the rat to evaluate the stimulation-induced electric field across the skull. This model, which includes both the skull and detailed brain structures, allowed us to align precisely the simulation geometry with the

physical setup, which was crucial for accurately modeling the magnetic field interaction with the brain. The rat CT images were acquired using a volumetric micro-CT scanner (NFR Polaris G90C, NanoFocusRay, Ikson, Korea). The image size was 1024×1024 pixels and 434 slices, and the size of the voxels was 0.0698×0.0698×0.1396 mm^3. Manual segmentation was made using Seg3d (NIH/NIGMS CIBS, University of Utah, UT, USA) [32] to guarantee continuity and to improve the accuracy of segmentation. The volume conduction model was constructed to include the scalp, skull, and brain. Lastly, the finite element model of the rat head was generated by an optimized tetrahedral mesh using the Iso2Mesh toolbox [33], TetGen [34], and Matlab. We used the Kodein toolbox to create the rectangular coil employed in this study [35] and SimNIBS version 4.0 (http://www.simnibs.org) [36] to simulate the AMF- induced electric field. In the simNIBS workflow, simulations begin by computing the change in the magnetic vector potential from the coil models, and the Kodein Box calculates the magnetic vector potential from user-defined coil path data. Simulation problems are then solved using the finite element method. The electrical properties of each tissue, which were taken from standard conductivity values from SimNiBS, were assigned as follows (S/m): skin: 0.465; skull: 0.01; brain: 0.275 [37].

D. Design of Magnetic Field Generation and Behavioral Testing Setup

Alternating magnetic fields were generated using custom-designed, water-cooled rectangular coil driven by a 5 kW power generator (Ultraflex Power Technology, Ronkonkoma, NY, USA), with an operational frequency range of 50–450 kHz. The coil assembly had a free aperture size of 12.7 × 4.75 mm and an overall length of ~320 mm. The system achieved a peak magnetic field of 14.5 kA/m, with a maximum current of 648 A at ~415 kHz, corresponding to 2594 ampere-turns as specified by the power supply. The current density was calculated as 10.8 A/mm^2, while the total inductance of the three parallel pancake windings was 1.01 μH. At maximum field, the total power consumption was ~270 W (RMS). Structurally, the coil consisted of four turns, providing an optimized balance between field strength and resistive losses. The dimension of rectangular coil was 96 mm x 82 mm x160 mm with the four turn structure designed to house the "behavioral testing box". Importantly, the novelty of the coil design does not lie in introducing a fundamentally new magnetic principle, but in enabling stable and behavior-compatible delivery of ultra-high-frequency, low-intensity magnetic stimulation (UHF-LiMS) in awake, task-engaged animals. The coil geometry is an original design developed, specifically tailored to accommodate both the anatomical scale of the rat head and the functional requirements of awake behavioral experiments. Rather than employing a uniformly wound or simply down-scaled circular coil, the winding distribution was deliberately configured to reduce dead space and to enhance magnetic field delivery within the brain-relevant region of the behavioral enclosure. The concentric rectangular layout further allows animals to perform tasks such as single-pellet reaching without obstruction, while maintaining stable magnetic field coupling to the target brain regions. This design therefore supports consistent stimulation under natural behavioral conditions. The magnetic field strength was first simulated based on coil design and validated by direct measurement of voltage from the nine probes placed in the fabricated fixture.

E. Ultra-high frequency low intensity magnetic stimulation

Consistent with our earlier studies [38], we confirmed persistent motor deficit for two weeks in all the experimental animals to ensure a reliable capsular infarct lesioning. Each animal was placed in a behavioral test box, which itself was positioned inside a water-cooled rectangular magnetic coil and only the experimental groups received magnetic stimulation. To determine the field strength of AMF for magnetic stimulation, we adjusted the strength (kA/m) and frequency (kHz) within physiologically safe ranges [39].

Three different magnetic fields strengths were generated (3 kA/m, 5 kA/m, and 10 kA/m) via AMF programmer. These magnetic strengths corresponded approximately to 3 mT, 5 mT and 10 mT, respectively. The stimulation protocol included 20 seconds of active stimulation followed by a 40 second rest period. This cycle of stimulation was repeated for 21 minutes while the animals underwent SPRT testing in the same manner as described above.

F. Behavioral Evaluation

All rats were trained on Single Pellet Reaching Task (SPRT) daily (pretraining period), before stimulation (following infarct lesioning) and during magnetic stimulation experiment. The SPRT was conducted in a box made of clear Plexiglas that measured (45 cm × 40 cm × 13 cm) with 1cm in the middle of front wall. A small food shelf was attached in front of the slit. The handedness of each rat was determined by evaluating how successful the rat's preferred paw was in retrieving sucrose pellets (Bio-Serve, Frenchtown, NJ) that had been placed on the shelf during the pre-training phase. The rats were given 20 pellets in twenty-one minute of session. Reaching performance was calculated as the percentage of successful retrieval of pellets according to following equation:

$$SPRT\ Score\ \% = \frac{Number\ of\ successful\ retrieval\ \times 100}{20}$$

G. Longitudinal Micro-Positron Emission Tomography Imaging Protocol and Evaluation

All animals in the control and experimental groups underwent longitudinal microPET scans to evaluate their regional glucose metabolism (rGM). The rats were subjected to four scans as follows: the baseline prior to infarct lesioning (baseline scan), two weeks following lesioning but before magnetic stimulation (PS-1), 7 days' post-stimulation (PS7) and 14 days' post-stimulation (PS14). Animals were deprived of food for 12 h and then injected with [18F]-FDG (0.1 mCi/100 g) through the tail vein under brief isoflurane anesthesia. After a thirty-minute uptake period, the rats were anesthetized again with 2% isoflurane and placed in a prone position on the microPET scanner (Siemens Medical Solutions, TN, USA) with a holder that was specifically fabricated to immobilize their heads (Hyosung Inc., Gwangju, Korea). We acquired a static

PET scan for 25 minutes and a CT scan with attenuation correction for 5 minutes. During the scan, the breathing rate (50±5 respirations/min) heart rate (280±20 beats/min) and core temperature (37.0±1 °C) were recorded and displayed on a computer (BioVet; m2m Imaging Corp, Newark, NJ, USA). After attenuation correction, the collected images were reconstructed using the three-dimensional ordered-subsets expectation maximum (3D-OSEM) technique, which included integrated scatter correction and random correction. The imaging data were analyzed using the MINC toolkit (McConnell Brain Imaging Centre, Montreal Neurological Institute, Canada) and the AFNI software suite (National Institutes of Health, Maryland, USA). Spatial normalization was performed to align all images to a standardized MRI template of the Sprague Dawley rat brain. Voxel intensities were then normalized to the average whole-brain intensity to ensure consistency across datasets. To improve spatial resolution and to reduce noise, the images were smoothed using an isotropic Gaussian kernel with a full width at half maximum (FWHM) of 1.2 mm.

H. Immunohistochemical Analysis

After two weeks of magnetic stimulation, animals were sacrificed and processed for immunohistochemical analysis. Briefly, rats were perfused with 0.9% saline and 4% paraformaldehyde (PFA) and coronal brain sections were prepared (40 µm) on a freezing microtome (Cryocut 3000, Leica Biosystems. Histological sections were prepared using Nissl staining and anti-GFAP staining (1:300, Millipore, AB5541). c-Fos labeling was used as a measure of brain activity (1:1000, Cell Signaling, 2250S). A cell density map of c-Fos expression was constructed using MATLAB (MathWorks, Natick, Massachusetts, United States) and ImageJ (https://imagej.nih.gov/ij/) as shown in our previous studies [40].

I. Statistical Analysis

FDG-microPET images were analyzed statistically with a group-level linear mixed-effect model (3dLME in AFNI). The image analysis compared prelesional (baseline) and post-lesional images (PS-1, PS7, and PS14) to identify longitudinal changes in cortical diaschisis and glucose metabolism by magnetic stimulation. Statistical maps were corrected and thresholded at the significance level ($p < 0.001$, false discovery rate $q < 0.05$). In addition, the image analysis compared the pre-stimulation (PS-1) and post-stimulation images (PS7 and PS14) to assess effects of magnetic stimulation. Statistical maps were thresholded at the significance level in AFNI ($\alpha = 0.05$, $p < 0.001$, $k < 39$) and the maps were superimposed on the MRI template, thus revealing regions with significant metabolic change.

To gain deeper insights into the brain regions exhibiting elevated metabolic activity, a Pearson's correlation map was constructed. Regions of interest (ROIs) were selected in the cortical areas, including the motor and sensory cortices, at PS7 and PS14 along the ipsilateral and contralateral sides. These ROIs were delineated using AFNI to ensure reliable analysis. Each section was segmented further to facilitate accurate and detailed analysis. For this analysis, positive voxel values from each activated region identified in the PET scans were used to calculate Pearson correlation coefficients with reaching score, enabling a quantitative assessment of the stimulation effected in the brain. Statistical analysis was performed using Prism 7 (GraphPad, San Diego, CA, USA). The association between changes in cortical diaschisis volume, NMA, and SPRT performances over time were analyzed using repeated-measures two-way ANOVA with Bonferroni post hoc test. In addition, the c-Fos data were analyzed using a two-way ANOVA followed by a Bonferroni post hoc test. This study employed Threshold-Free Cluster Enhancement (TFCE) analysis to examine the volume of individual clusters in regions with elevated metabolic activity, utilizing the MRIcroGL software. To analyze infarct volume, an analysis of variance followed by Tukey's test was used. Using linear regression ($p=0.05$), correlations between NMA and SPRT scores were assessed, and changes in NMA or diaschisis volume were compared to SPRT scores. The information is given as a mean and standard deviation (S.E.M.). Asters denote significance ((*$p<0.05$), (**$p<0.01$), (***p0.001), (****$p<0.0001$) and ns, not significant) respectively.

IV. Results

A. Optimization of a magnetic field setup and preliminary effect

The magnetic stimulation system consists of a programmable power supply, a cooled-water-based magnetic field generator, and a custom fabricated magnetic coil (Fig. 1a). The coil, with four rectangular turns and an open architecture, was specifically engineered to facilitate unrestrained stimulation of awake rats without requiring anesthesia. Also, its geometry emphasizes a stronger peripheral magnetic field relative to the central region (0,0,0). Three distinctive stimulation intensities 3 mT, 5 mT and 10 mT were implemented with a standardized stimulation protocol (Fig. 1b). The system specifications are detailed in the Materials and Methods section under "Design of Magnetic Field Generation and Behavioral Testing Setup". The coil measures 96 mm x 82 mm x 160 mm, as depicted in (Fig. S1a). To enhance the field orientation near the anterior and posterior ends of the device coil, winding density was increased in these regions.

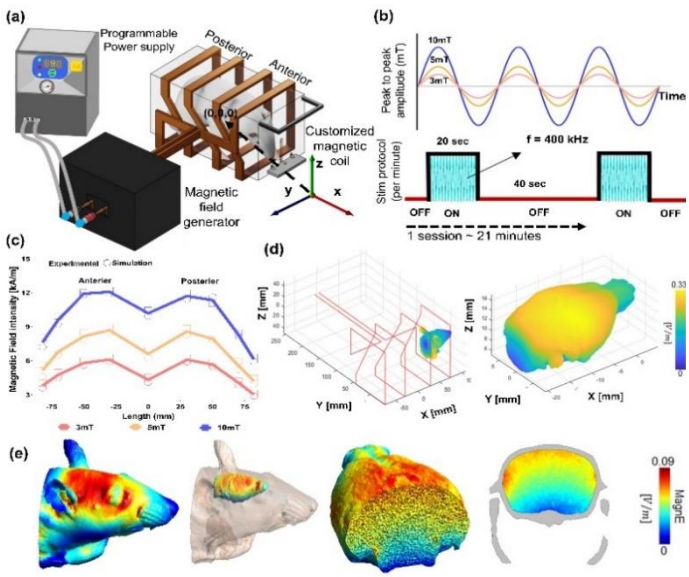

Fig. 1. Experimental setup and electromagnetic field characterization of UHF-LiMS. (a) Schematic of the stimulation setup comprising a programmable supply, magnetic generator, and custom four-turn coil. (b) Illustration of stimulation waveforms at 3, 5, and 10 mT at 400 kHz frequency, with a 20 s ON / 40 s OFF cycle repeated for ~21 min. (c) Experimental and simulated magnetic field profiles along the coil's central axis (150 mm, anterior–posterior) showing symmetric distribution and intensity-dependent peaks. (d) Simulated 3D distribution of magnetic and induced electric fields in a rat head model (skull + brain) positioned at the periphery. (e) FEM simulations depicting the induced electric field distribution within the brain, with heatmaps showing field penetration and localization across anatomical views.

A 3D-printed fixture with nine spatially distributed measurement points, approximating the in vivo rat brain position was used to optimize field uniformity (Fig. S1b). Magnetic flux density was derived from oscilloscope voltage readings converted to magnetic field intensity (A/m) following the procedure outlined in "Calculation of Manual Magnetic Field" of the Supplementary Text. With the coil current at 528A_{RMS}, the magnetic field strength was mapped longitudinally, revealing deviations in the anterior and posterior (Fig. 1c). These peaks correspond to coil turns, whereas field minima (troughs) were found between the turns. To verify our experimental observations, computer simulations using ANSYS HFSS and a SOLIDWORKS modeled coil were performed. Simulated distributions showed strong concordance with experimental results across all tested intensities (Fig. 1c). The in vivo positioning of the rat brain during stimulation was digitally co-registered with a 3D head model encompassing the skull and brain (Fig. S1c). Simulations of induced electric fields were performed using the SimNIBS platform and a coil model from the Kaiserslautern Coil Design Instrument (Kodein). When placed at the center coil (Fig. S1d) and anterior (Fig. 1d) respectively, our results showed greater induced electrics at the periphery, highlighting the non-uniform distribution of the electric filed.

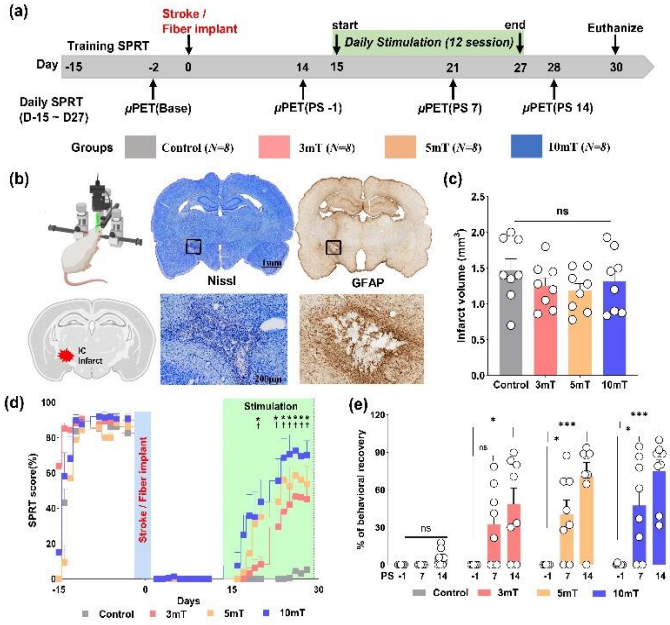

Fig. 2. (a) Experimental timeline: SPRT training (−15 to 0), stroke induction (0), stimulation (15–27), and FDG-μPET at baseline, PS−1, PS7, and PS14. (b) Schematic of stroke targeting the internal capsule (IC) with histological validation: Nissl staining shows infarct boundaries, and GFAP staining reveals lesion-core gliosis. (c) Quantification of infarct volume shows no significant differences between groups (one-way ANOVA, $F_{(3, 28)} = 0.8681$, $p = 0.4693$). (d) Daily success rate across all groups. Shaded green region indicates the stimulation period. Statistical analysis via two-way RM ANOVA ($F_{(90, 840)} = 7.016$, $p < 0.0001$). (e) Percentage recovery relative to pre-lesional performance, showing significant behavioral restoration in the 5 mT and 10 mT groups by PS14 (two-way ANOVA, $F_{(2, 21)} = 48.70$, $p < 0.0001$). All bar graphs represent mean ± SEM. Significance determined by Tukey's multiple comparison test (*$p < 0.05$, **$p < 0.01$, ***$p < 0.001$, ****$p < 0.0001$).

Finite Element Method (FEM) simulations corroborated these findings, indicating lower central electric field magnitudes (Fig. S1e) compared to the periphery (Fig. 1e). To assess the simulation effects in vivo, cohorts of naïve rats (see section "Animals"), who received no prior exposure to magnetic fields or behavioral training were used. The stimulation timeline (Fig. S2a) and protocol is provided in the supplementary text, under the section "Naïve Animal Study (Timeline)". FDG-microPET imaging revealed bilateral cortical glucose hypermetabolism relative to subcortical areas, consistent with the predictions from our model (Fig. S2b). 3D rendering representation of activated clusters confirmed widespread engagement across the cortical regions (Fig. S2c). Further c-Fos expression by immunohistochemical analysis demonstrated elevated neuronal activity at the cellular level in all stimulation groups (Fig. S2d). Together, these experimental and computational analyses confirm that UHF-LiMS delivers spatially heterogeneous fields that can preferentially engage cortical networks, proving its utility in neurostimulation.

B. UHF-LiMS enhances behavioral recovery in stroke model

The detailed experimental timeline and procedures are illustrated in (Fig. 2a) with detailed group information available in the supplementary text under "Stroke Animals Study (Timeline)". A total of 32 rats were assigned to four groups as follows: control, 3 mT, 5 mT, and 10 mT. We performed chronic photothrombotic capsular infarct surgery on all animals, which led to persistent motor deficits approximately 14 days' post-induction of stroke, consistent with established stroke models [38, 41].

Additionally, the infarct was localized to the internal capsule as confirmed by Nissl and GFAP staining (Fig. 2b). To assess motor recovery, single pellet reaching task (SPRT) (see "Behavioral Evaluation"), a validated assay for evaluating fine motor function following subcortical injury was employed [38]. Lesion volumes across groups were also quantified (Fig. 2c). All animals were evaluated across three sequential stages including: pre-training, stroke induction and magnetic stimulation. The behavioral assessment setup during the stimulation phase is depicted in (Fig. S3a). Across all the stimulation timepoints, animals in all UHF-LiMS treated groups exhibited significant improvement in forelimb function, while the control group animals failed to show meaningful recovery. During the first week of stimulation, all treatments groups showed a progressive performance increase in SPRT performance, in contrast to the stagnation observed in the control group (Fig. 2d). Response rates in the stimulation groups ranged from 50% to 85% in both dominant and non-dominant limbs (see Videos 1 and 2). To quantify recovery, the "first reach success rate" was analyzed at post-stimulation days 7 and 14 (PS7 and PS14) (Fig. S3b) and showed a significant increase in reaching success for all stimulated groups, with greater gains observed in the higher intensity conditions (5 mT and 10 mT). Moreover, when normalized to pre-lesion performance, the overall success of behavioral recovery was substantially greater in all UHF-LiMS groups compared to the control (Fig. 2e). Notably, the 10 mT group exhibited the best recovery thus establishing a dose-dependent relationship between stimulation intensity and motor improvement. (see Videos 3 and 4).

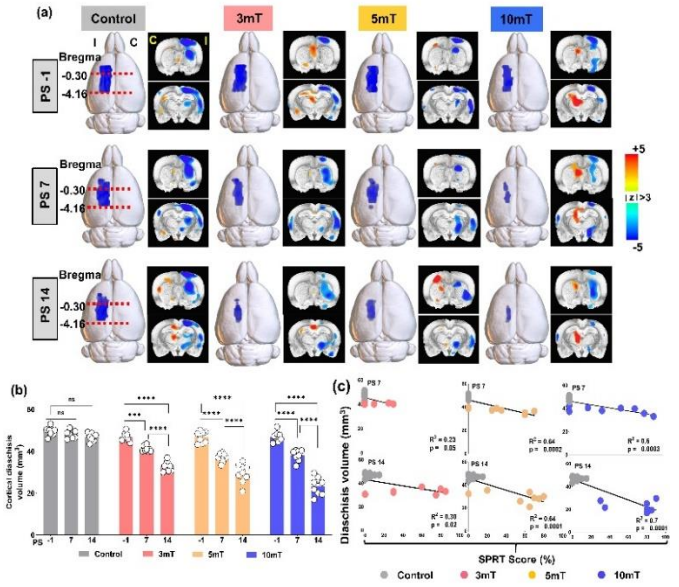

Fig. 3. (a) Longitudinal FDG-μPET imaging showing 3D reconstructions and coronal slices across experimental groups (Control, 3mT, 5mT, 10mT) at post-stimulation day 1 (PS-1), day 7 (PS7), and day 14 (PS14). Time-dependent changes in cortical diaschisis were evaluated by image analysis (3dLME in AFNI, p=0.001, q < 0.05 FDR corrected). The color scale bar represents z-scores, with positive values (orange–red) indicating increased glucose metabolism relative to baseline, and negative values (blue) indicating decreased metabolism. I, ipsilesional; C, contralesional. (b) Quantification of diaschisis volume across time points. UHF-LiMS reduced diaschisis volume in a field strength- and time-dependent manner (Two-way ANOVA, $F_{(6,84)} = 21.93$, $p < 0.0001$). (c) Cortical diaschisis volume was inversely associated with SPRT score among stimulated groups (3 mT, 5 mT 10 mT) at PS7 (($F_{(1,14)} = 4.219$), ($F_{(1,14)} = 25.43$), ($F_{(1,14)} = 20.58$)), and at PS14 (($F_{(1,14)} = 6.132$), ($F_{(1,14)} = 31.12$), ($F_{(1,14)} = 49.50$)) respectively.

C. UHF-LiMS induces metabolic changes after stroke

Following ischemic stroke, widespread alterations in neural activity are frequently observed in regions distant from the infarct core, a phenomenon known as diaschisis (see section "Induction of Photothrombotic Capsular Infarction"). Diaschisis is characterized by decreased metabolic activity in functionally connected areas and is, considered a biomarker of disrupted inter-regional communication and a target for rehabilitation therapies [38, 42]. In previous studies, both electrical stimulation and intensive rehabilitative training were shown to significantly reduce diaschisis volume and leading to enhanced motor recovery [43, 44]. We have demonstrated previously that diaschisis in this model is mediated in part by reactive astrocytes, which produce tonic GABAergic inhibition in cortical areas remote from the infarct, thus suppressing neuronal excitability [45]. To assess the effect of UHF-LiMS on diaschisis we conducted longitudinal [18F]-FDG-microPET imaging, with four scans per animal (Fig. 3a). A baseline scan was performed pre-lesion, along with scans on day 14 post-infarct (PS-1) prior to stimulation onset and two follow-up scans on day 7 and 14 after the initiating stimulation (PS7 and PS14). Full imaging details are provided in the section under "Longitudinal Micro-Positron Emission Tomography Imaging

Protocol and Evaluation". Significant reductions in the cortical diaschisis volume were observed in all stimulated groups at PS7 and PS14 (Fig. 3b), but not in the control group. Importantly, the reduction in diaschisis volume was strongly correlated with improved motor performance, as measured by SPRT scores at both stimulation time points (Fig. 3c). In contrast control animals failed to exhibit either a reduced diaschisis or behavioral gains. Normalized mean activity (NMA) in the cortical diaschisis region was also analyzed. While NMA declined in the control animals compared to baseline (Fig. S3c), stimulated groups demonstrated a gradual and robust increase in cortical NMA over the stimulation timepoint and is, evident at PS7 and PS14. This trend was consistent across all magnetic field strengths studied (3 mT,5 mT and 10 mT). A positive correlation between SPRT and cortical NMA was confirmed for all stimulation groups at both timepoints (Fig. S2d), underscoring the tight link between metabolic restoration and behavioral recovery. Collectively, these results indicate that UHF-LiMS effectively mitigated, diaschisis, likely through the restoration of cortical excitability and inter-regional connectivity. In conclusion, the modulation of metabolic activity in neural cells by UHF-LiMS plays a crucial role in functional recovery post-stroke, supporting its potential as a non-invasive therapeutic strategy to enhance regional glucose metabolism (rGM) and motor outcomes [46].

D. Spatial distribution of brain activation with UHF-LiMS

To further characterize the neural effects of stimulation, we analyzed [18F]-FDG microPET images to assess changes in brain metabolic activity following UHF-LiMS across all treatment groups (Fig. 4). The goal was to provide a spatially resolved overview of brain activation and to determine how the stimulation modulates neuronal activity over time (Fig. 4a), displays representative coronal sections from the animals in each experimental group at post-stimulation days 7 and 14 (PS7 and PS14). Across all UHF-LiMS groups, FDG uptake was increased bilaterally in both motor and sensory cortices compared to the control group, indicating enhanced cortical metabolic activity. In particular, animals in the 5 mT and 10 mT groups showed FDG accumulation in both the cortical and subcortical regions, (including thalamus and hippocampus), an effect that was less prominent in the 3 mT group. These finding suggest that higher magnetic field intensities broaden the activation footprint, potentially by engaging deeper neural structures [44, 47]. We quantified (Fig. 4b-e) the volumes of activated clusters at PS7 and PS14 and respective ROI correlation, demonstrating a clear dose-dependent relationship between stimulation intensity and the extent of activation. This includes a larger number of activated positive voxels and a higher spatial spread in the higher intensity groups (particularly at 10 mT).

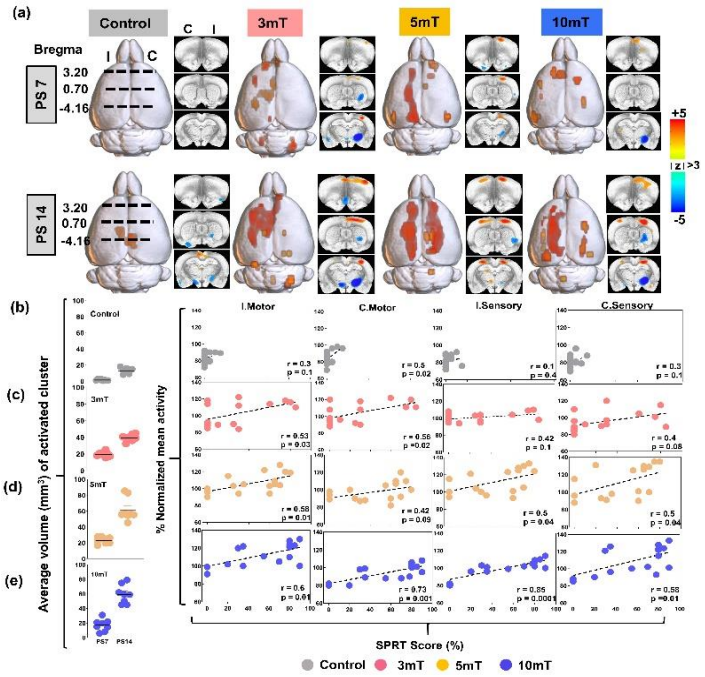

Fig. 4. (a) 3D-rendered FDG-microPET images with color-coded map depicting the cortico-cortico and cortico-subcortico activation as a result of UHF-LiMS. Time-dependent metabolic changes in brain activation were evaluated by image analysis (3dLME in AFNI, $p = 0.001$, FDR $q < 0.05$) by comparing pre- and post-stimulation images. I, ipsilesional; C, contralesional. (b) Group-wise average volume of activated clusters (mm^3) across time points of control group and Pearson's correlation between different brain regions and behavior score, I. Motor ($_{(F\,(1,14)} = 2.012$), C. Motor ($F_{(1,14)} = 6.044$), I. Sensory ($F_{(1,14)} = 0.5597$), C. Sensory ($F_{(1,14)} = 1.82$)). (c) Group-wise average volume of activated clusters at PS7 and PS14 of 3mT and corresponding correlation with behavior score, I. Motor (($F_{(1,14)} = 5.71$), C. Motor ($F_{(1,14)} = 6.62$), I. Sensory ($F_{(1,14)} = 3.029$), C. Sensory ($F_{(1,14)} = 3.52$)). (d) Average activated volume of 5mT group brain regions and Pearson's correlation with respect to SPRT score, I. Motor (($F_{(1,14)} = 7.41$), C. Motor ($F_{(1,14)} = 3.152$), I. Sensory ($F_{(1,14)} = 3.275$), C. Sensory ($F_{(1,14)} = 3.194$)). (e) Average volume of activated cluster in 10mT group corresponding correlation with behavior score, I. Motor (($F_{(1,14)} = 8.596$), C. Motor ($_{F\,(1,14)} = 16.85$), I. Sensory ($F_{(1,14)} = 38.10$), C. Sensory ($F_{(1,14)} = 7.413$)) respectively.

To establish a relationship between these metabolic changes and functional recovery, we performed region-of-interest (ROI) analyses to find the correlation between changes in glucose metabolism and behavioral performance. Positive voxel counts within defined cortical ROIs were used to compute the correlations with SPRT scores. Stimulated groups showed a strong and significantly positive correlation between metabolic enhancement and reaching success at both PS7 and PS14 across both hemispheres. In contrast, no significant correlation was observed in the control group, confirming that the observed functional improvements were specifically associated with stimulation-induced metabolic shifts. Finally, a clear dose-response trend was evident as higher UHF-LiMS intensities corresponded to larger volumes and stronger correlations with behavioral gains (Fig. 4e). This reinforces our interpretation that UHF-LiMS promotes neural plasticity in a dose-dependent manner, enhancing both functional integration and coordination across brain regions. Collectively, these findings suggest that

UHF-LiMS promotes network-level reorganization which underlies its therapeutic benefit in stroke rehabilitation [48].

E. UHF-LiMS instigates pervasive c-Fos expression

To assess the impact of UHF-LiMS on neuronal activation at the cellular level, we quantified c-Fos protein expression, a widely accepted marker of neuronal depolarization and activity-dependent genes [49] (Fig. 5). The procedures of this analysis are detailed under "Immunohistochemical analysis" of the Materials and Methods section. Minimal c-Fos expression was observed in the control group reflecting limited neuronal activation in the absence of stimulation. In contrast, all stimulated groups (3 mT, 5 mT and 10 mT) exhibited robust and widespread in c-Fos expression, within the ipsilesional and contralesional sensory cortex (Fig. 5a). This upregulation in c-Fos expression confirms that magnetic stimulation elicited strong neuronal activity across bilateral brain regions. The magnitude and distribution of c-Fos expression differed significantly between the control and stimulation groups, as visualized in the density heatmaps (Fig. 5b). The expression was widely distributed across cortical regions, including the motor cortex, sensory cortex, cingulate gyrus and striatum, suggesting global bilateral neuromodulatory effects of UHF-LiMS (Fig. 5c).

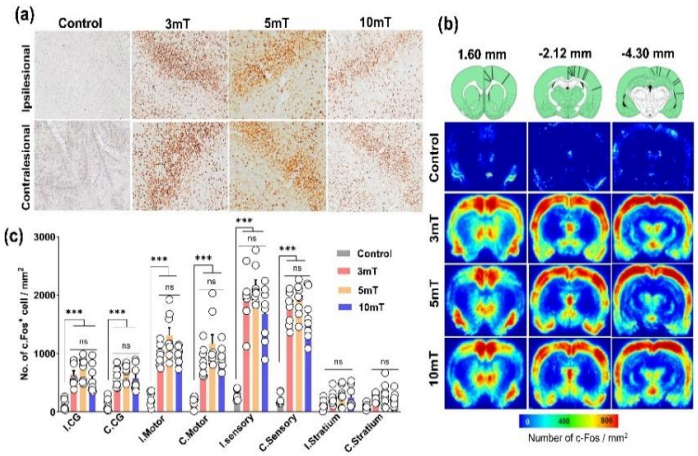

Fig. 5. (a) Representative c-Fos immunostaining in coronal sections from control and stimulated (3, 5, 10 mT) groups showing increased expression in the sensory cortex of both hemispheres. (b) Heatmap visualization of c-Fos–positive cell density across the brain. Maps are overlaid on standard rat atlas levels (Bregma +1.60 mm, −2.12 mm, −4.30 mm). (c) Quantification of c-Fos–positive cell density across bilateral cingulate gyrus, motor cortex, sensory cortex, and striatum. UHF-LiMS groups exhibited significant upregulation compared to control (Two-way ANOVA, $F_{(21,216)} = 11.44$, $p < 0.0001$; Bonferroni post hoc: *$p < 0.03$, **$p < 0.007$, ***$p < 0.0001$). Each dot represents a single animal.

This widespread c-Fos activation pattern is reminiscent of responses previously observed with prolonged electrical stimulation where both hemispheres showed increased neuronal activity [43]. These findings demonstrate that UHF-LiMS can achieve a comparable effect to electrical stimulation therefore reinforcing its utility for non-invasive neruomodulation. In addition to increased neuronal activity, UHF-LiMS also exhibited neuroprotective effects, as indicated by a reduction in apoptotic cells in both the ipsilesional (Fig. S3a) and contralesional sensory cortex (Fig. S3b) [50, 51]. TUNEL staining demonstrated that all three stimulation intensities significantly reduced cell death, indicating that UHF-LiMS attenuates neurotoxic processes and promotes cellular viability. Taken together, these data suggest that UHF-LiMS promotes stimulation-induced activity across broad brain territories, with the expression of immediate early genes like c-Fos serving as a biomarker for activity-dependent plasticity. Furthermore, the bilateral enhancement of c-Fos expression and reduction in apoptosis underscore the therapeutic potential of UHF-LiMS for facilitating functional and structural recovery after stroke.

IV. Discussion

Traditionally, rTMS and TMS relied on brief, high-intensity pulsed waveforms to induce rapid neuronal depolarization [52]. However, this approach has several limitations, including discomfort, pain, and the risk of overstimulation, which arises from the abrupt modulation of neuronal circuits [53]. These concerns are particularly crucial when considering treatment options in vulnerable or neurologically impaired populations [19]. To overcome these limitations, alternative treatment paradigms such as low-intensity TMS using sinusoidal waveforms have gained popularity. These waveforms can provide gentler and, more sustained neuronal modulation, thereby enhancing tolerability and therapeutic benefits [54]. Evidence from alternating current stimulation (tACS), supports the notion, that sinusoidal fields can entrain neural oscillations and modulate large-scale networks [55]. Although sinusoidal magnetic stimulation is less-well explored in the context of TMS, it holds strong, theoretical promise for safe and rhythmic modulation of brain activity. Here, we introduce a novel approach called, ultra high frequency low-intensity magnetic stimulation (UHF-LiMS), which involves the application of 400 kHz sinusoidal fields of between 3 to 10mT in a rat model of chronic internal capsule stroke. The stimulation frequency of 400 kHz was selected based on the system's optimal operating field range, reflecting a trade-off between achievable magnetic field amplitude, physiological safety limits, and hardware stability. As reported [39], frequencies in the range of 350–400 kHz allow effective low-intensity field delivery (~0.012–0.015 T) while remaining below recommended physiological and thermal constraints.

This strategy led to remarkable functional recovery, a result that is often difficult to achieve in subcortical stroke models [56]. Compared to conventional pulsed TMS, which primarily uses monophasic or biphasic waveforms, UHF-LiMS provided consistent therapeutic effects over time and achieved superior behavioral outcomes, most notably in forelimb motor function and diaschisis [57]. Importantly, the induced electric fields generated by UHF-LiMS (~0.1 V/m) are well below thresholds required for direct neuronal depolarization or spike initiation, and thus the observed effects are unlikely to arise from direct electrical excitation. Instead, UHF-LiMS is best interpreted within a framework of subthreshold neuromodulation, in which weak fields bias ongoing cellular and network dynamics rather than driving spiking activity directly. Sensitivity to weak

magnetic fields has been documented even in non-neural systems such as bacteria [58], which lack excitable membranes, where low-intensity fields influence cellular behaviour via modulation of spin-dependent biochemical reactions, including radical pair mechanisms [59]. Within neural circuits, analogous weak-field interactions may subtly modulate synaptic integration and membrane potential fluctuations in neurons operating near threshold. When delivered repeatedly and during active task engagement, such subthreshold perturbations can be amplified at the network level through recurrent connectivity and activity-dependent plasticity, providing a mechanistic basis for the sustained behavioural and metabolic effects observed here.

We propose that UHF-LiMS could serve as a viable alternative to high-intensity TMS and other neuromodulation techniques when used in post-stroke rehabilitation. A distinctive strength of this approach lies in the experimental design. Animals were fully conscious and actively engaged in the single pellet-reaching task during the stimulation, avoiding the confounding effects of anesthesia and offering real-time behavioral assessment of neuromodulation efficacy. Behavioral data confirmed that UHF-LiMS did not induce any adverse effects as there were no significant behavioral differences between control animals with or without stimulation. Given the severity of capsular infarcts, animals were already in a vulnerable state and applying high magnetic field strength might have exacerbated any prior damage. Our decision to use low-intensity fields was grounded in safety considerations to minimize tissue damage and discomfort. Although a direct comparison with conventional rTMS would be informative, such an analysis was beyond the scope of the present study. Importantly, UHF-LiMS differs fundamentally from high-intensity rTMS in stimulation intensity and compatibility with task engagement. While higher-intensity rTMS can modulate motor learning, it often induces involuntary muscle contractions and mechanical artifacts that would interfere with skilled motor tasks in awake animals [18,19]. In contrast, UHF-LiMS enables low-intensity, task-engaged stimulation during fine motor behavior, making it well suited for the rehabilitation paradigm examined here [60].

The chronic stroke model we employed induces motor deficits that persist for more than 3 months, closely mimicking long-term human stroke disability. This made it an ideal platform to explore the potential for non-invasive neuromodulatory therapies like UHF-LiMS. Functional brain imaging via microPET revealed that UHF-LiMS reversed cortical diaschisis and restored metabolic activity in remote but interconnected cortical areas. As demonstrated in previous studies, diaschisis reflects disrupted network function, often driven by tonic GABA release from reactive astrocytes that inhibit neurons [45]. Our imaging data confirmed that stimulation normalized these metabolic deficits and was correlated with behavioral improvement. Notably, the spatial distribution of metabolic activation differed across stimulation amplitudes, with 3 mT producing weaker effects, 5 mT predominantly enhancing cortical activity, and higher-intensity stimulation also engaging subcortical regions. Despite these spatial differences, functional recovery was comparable at ≥5 mT, supporting a threshold-dependent rather than linear amplitude-efficacy relationship. At the cellular level, UHF-LiMS robustly increased c-Fos expression, a key marker of neural activation and plasticity [61] in both hemispheres, indicating widespread cortical and subcortical engagement. This aligns with the bilateral activation patterns observed in our FDG-microPET data, further validating the global network-level effect of the intervention. Additionally, TUNEL assays revealed a significant reduction in apoptosis, suggesting that UHF-LiMS confers neuroprotective benefits in addition to its plasticity-promoting effects [50, 51]. To our knowledge, ours is the first study to demonstrate that ultra-high frequency, low-intensity sinusoidal magnetic stimulation can modulate brain metabolism and behavior in a chronic stroke model. Looking ahead, we propose a translational framework for UHF-LiMS applications in humans. One concept involves a “magnetic room” in which field strength varies spatially, emulating the gradient generated by a dynamic coil. From a practical perspective, localized coil-based systems offer advantages in terms of portability, cost, and ease of implementation. In contrast, room-scale or large-area coil configurations may provide improved freedom of movement during task-specific rehabilitation, eliminate direct head contact, and enable more uniform field exposure during prolonged stimulation sessions. However, such room-scale approaches also introduce challenges related to infrastructure requirements, installation complexity, and cost, which must be carefully weighed against their potential benefits. Nonetheless, the translational gap between rodent and human studies remains a major hurdle. Anatomical and physiological differences such as brain volume, gyrification, and circuit organization may limit direct extrapolation. Therefore, replication in non-human primates will be essential to validate our findings and to assess the safety, tolerability, and dose parameters in a species closer to humans. In conclusion, UHF-LiMS offers a promising non-invasive, well-tolerated, and scalable strategy for post-stroke rehabilitation. Future studies will aim to optimize stimulation protocols, further characterize mechanistic pathways, and explore clinical translation in larger animal models.

V. Conclusion

In summary, this study introduces Ultra High Frequency Low-Intensity Magnetic Stimulation (UHF-LiMS) as a novel non-invasive brain stimulation approach demonstrating significant functional recovery from motor deficits and reduced diaschisis in a rat stroke model. To our knowledge this study provides the first evidance that UHF-LiMS, utilizing a unique combination of frequency and intensity, can modulate metabolic activity across multiple brain regions and enhance neural plasticity. Our findings support the potential of UHF-LiMS therapy as a promising and tolerable approach for post-stroke rehabilitation, opening new therapeutic options that could be competitive with traditional TMS. The sustained functional improvements observed in conscious animals warrant further investigation into its safety and efficacy for translation to human clinical applications.

ACKNOWLEDGMENT

We express our gratitude to Prof. Youngjoo Chung for providing valuable guidance in the design of the coil, Prof. Jung Won Yoon for assistance with magnetic field validation process, Mr. H.U. Rehman for support in the simulation study, and Dr. Michael Ye for helpful discussions and assistance in improving the clarity of the manuscript.

REFERENCES

[1] T. M. Markus, S. Y. Tsai, M. R. Bollnow, R. G. Farrer, T. E. O'Brien, D. R. Kindler-Baumann, M. Rausch, M. Rudin, C. Wiessner, and A. K. Mir, "Recovery and brain reorganization after stroke in adult and aged rats," *Annals of Neurology: Official Journal of the American Neurological Association and the Child Neurology Society*, vol. 58, no. 6, pp. 950-953, 2005.

[2] M. B. Bevers, J. An, A. Yoo, E. Fietsam, C. Booraem, D. Reddy, K. Li, C. Sastre, A. Acharjee, and K. Sugimoto, "Brain Endothelial Soluble ST2 Production and Cerebral Edema in a Rat Model of Ischemic Stroke," *Annals of Neurology*, 2025.

[3] V. L. Feigin, M. Brainin, B. Norrving, S. Martins, R. L. Sacco, W. Hacke, M. Fisher, J. Pandian, and P. Lindsay, "World Stroke Organization (WSO): global stroke fact sheet 2022," *International journal of stroke*, vol. 17, no. 1, pp. 18-29, 2022.

[4] M. Katan, and A. Luft, "Global burden of stroke." pp. 208-211.

[5] L. R. Draaisma, M. J. Wessel, and F. C. Hummel, "Non-invasive brain stimulation to enhance cognitive rehabilitation after stroke," *Neuroscience letters*, vol. 719, pp. 133678, 2020.

[6] G. Cai, C. Zhang, J. Xu, J. Jiang, G. Chen, J. Chen, Q. Liu, G. Xu, and Y. Lan, "Efficacy of Transcranial Magnetic Stimulation in Post-Stroke Motor Recovery: Impact of Impairment Severity," *IEEE Transactions on Neural Systems and Rehabilitation Engineering*, 2025.

[7] H. Song, Y. Zeng, L. Ren, H. Zhang, A. Wang, J. Sun, and S. Tong, "Low-intensity Transcranial Ultrasound Stimulation Promotes Recovery in Blood Flow and Movement Following Prolonged Anesthesia," *IEEE Transactions on Neural Systems and Rehabilitation Engineering*, 2025.

[8] N. Jarrassé, T. Proietti, V. Crocher, J. Robertson, A. Sahbani, G. Morel, and A. Roby-Brami, "Robotic exoskeletons: a perspective for the rehabilitation of arm coordination in stroke patients," *Frontiers in human neuroscience*, vol. 8, pp. 947, 2014.

[9] E. C. Meyers, B. R. Solorzano, J. James, P. D. Ganzer, E. S. Lai, R. L. Rennaker, M. P. Kilgard, and S. A. Hays, "Vagus nerve stimulation enhances stable plasticity and generalization of stroke recovery," *Stroke*, vol. 49, no. 3, pp. 710-717, 2018.

[10] A. Tosun, S. Türe, A. Askin, E. U. Yardimci, S. U. Demirdal, T. Kurt Incesu, O. Tosun, H. Kocyigit, G. Akhan, and F. M. Gelal, "Effects of low-frequency repetitive transcranial magnetic stimulation and neuromuscular electrical stimulation on upper extremity motor recovery in the early period after stroke: a preliminary study," *Topics in stroke rehabilitation*, vol. 24, no. 5, pp. 361-367, 2017.

[11] C. Boake, E. A. Noser, T. Ro, S. Baraniuk, M. Gaber, R. Johnson, E. T. Salmeron, T. M. Tran, J. M. Lai, and E. Taub, "Constraint-induced movement therapy during early stroke rehabilitation," *Neurorehabilitation and neural repair*, vol. 21, no. 1, pp. 14-24, 2007.

[12] M. E. Gunduz, B. Bucak, and Z. Keser, "Advances in stroke neurorehabilitation," *Journal of clinical medicine*, vol. 12, no. 21, pp. 6734, 2023.

[13] F. J. Sanchez-Cuesta, Y. Gonzalez-Zamorano, A. Arroyo-Ferrer, M. Moreno-Verdu, and J. P. Romero-Munoz, "Repetitive transcranial magnetic stimulation of primary motor cortex for stroke upper limb motor sequelae rehabilitation: A systematic review," *NeuroRehabilitation*, vol. 52, no. 3, pp. 329-348, 2023.

[14] J. Veldema, and A. Gharabaghi, "Non-invasive brain stimulation for improving gait, balance, and lower limbs motor function in stroke," *Journal of NeuroEngineering and Rehabilitation*, vol. 19, no. 1, pp. 84, 2022.

[15] A. Pascual-Leone, J. M. Tormos, J. Keenan, F. Tarazona, C. Cañete, and M. D. Catalá, "Study and modulation of human cortical excitability with transcranial magnetic stimulation," *Journal of clinical neurophysiology*, vol. 15, no. 4, pp. 333-343, 1998.

[16] V. Di Lazzaro, F. Capone, F. Apollonio, P. A. Borea, R. Cadossi, L. Fassina, C. Grassi, M. Liberti, A. Paffi, and M. Parazzini, "A consensus panel review of central nervous system effects of the exposure to low-intensity extremely low-frequency magnetic fields," *Brain stimulation*, vol. 6, no. 4, pp. 469-476, 2013.

[17] M. L. Rohan, R. T. Yamamoto, C. T. Ravichandran, K. R. Cayetano, O. G. Morales, D. P. Olson, G. Vitaliano, S. M. Paul, and B. M. Cohen, "Rapid mood-elevating effects of low field magnetic stimulation in depression," *Biological psychiatry*, vol. 76, no. 3, pp. 186-193, 2014.

[18] C. M. Buetefisch, L. Wei, X. Gu, C. M. Epstein, and S. P. Yu, "Neuroprotection of Low-Frequency Repetitive Transcranial Magnetic Stimulation After Ischemic Stroke in Rats," *Annals of neurology*, vol. 93, no. 2, pp. 336-347, 2023.

[19] S. Rossi, A. Antal, S. Bestmann, M. Bikson, C. Brewer, J. Brockmöller, L. L. Carpenter, M. Cincotta, R. Chen, and J. D. Daskalakis, "Safety and recommendations for TMS use in healthy subjects and patient populations, with updates on training, ethical and regulatory issues: Expert Guidelines," *Clinical Neurophysiology*, vol. 132, no. 1, pp. 269-306, 2021.

[20] I. C. o. N.-I. R. Protection, "Guidelines for limiting exposure to time-varying electric, magnetic, and electromagnetic fields (up to 300 GHz)," *Health physics*, vol. 74, no. 4, pp. 494-522, 1998.

[21] L. Labruna, C. Merrick, A. V. Peterchev, B. Inglis, R. B. Ivry, and D. Sheltraw, "Kilohertz transcranial magnetic perturbation (kTMP) as a new non-invasive method to modulate cortical excitability," *Elife*, vol. 13, pp. RP92088, 2025.

[22] A. D. Tang, I. Hong, L. J. Boddington, A. R. Garrett, S. Etherington, J. N. Reynolds, and J. Rodger, "Low-intensity repetitive magnetic stimulation lowers action potential threshold and increases spike firing in layer 5 pyramidal neurons in vitro," *Neuroscience*, vol. 335, pp. 64-71, 2016.

[23] M. S. Markov, "Expanding use of pulsed electromagnetic field therapies," *Electromagnetic biology and medicine*, vol. 26, no. 3, pp. 257-274, 2007.

[24] I. Gunay, and T. Mert, "Pulsed magnetic fields enhance the rate of recovery of damaged nerve excitability," *Bioelectromagnetics*, vol. 32, no. 3, pp. 200-208, 2011.

[25] S. Di Loreto, S. Falone, V. Caracciolo, P. Sebastiani, A. D'Alessandro, A. Mirabilio, V. Zimmitti, and F. Amicarelli, "Fifty hertz extremely low-frequency magnetic field exposure elicits redox and trophic response in rat-cortical neurons," *Journal of cellular physiology*, vol. 219, no. 2, pp. 334-343, 2009.

[26] R. Piacentini, C. Ripoli, D. Mezzogori, G. B. Azzena, and C. Grassi, "Extremely low-frequency electromagnetic fields promote in vitro neurogenesis via upregulation of Cav1-channel activity," *Journal of cellular physiology*, vol. 215, no. 1, pp. 129-139, 2008.

[27] T. Dufor, S. Grehl, A. Tang, M. Doulazmi, M. Traoré, N. Debray, C. Dubacq, Z.-D. Deng, J. Mariani, and A. Lohof, "Neural circuit repair by low-intensity magnetic stimulation requires cellular magnetoreceptors and specific stimulation patterns," *Science advances*, vol. 5, no. 10, pp. eaav9847, 2019.

[28] S. Shin, H. Kim, and J. Jeong, "High-Frequency Magnetic Pulse Generator for Low-Intensity Transcranial Magnetic Stimulation," *Electronics*, vol. 13, no. 16, pp. 3160, 2024.

[29] J. Higgins, L. Koski, and H. Xie, "Combining rTMS and task-oriented training in the rehabilitation of the arm after stroke: a pilot randomized controlled trial," *Stroke research and treatment*, vol. 2013, no. 1, pp. 539146, 2013.

[30] W. Yan, Y. Lin, Y.-F. Chen, Y. Wang, J. Wang, and M. Zhang, "Enhancing neuroplasticity for post-stroke motor recovery: mechanisms, models, and neurotechnology," *IEEE Transactions on Neural Systems and Rehabilitation Engineering*, 2025.

[31] A. Evancho, W. J. Tyler, and K. McGregor, "A review of combined neuromodulation and physical therapy interventions for enhanced neurorehabilitation," *Frontiers in human neuroscience*, vol. 17, pp. 1151218, 2023.

[32] H. Seo, M. Han, J.-r. Choi, S. Kim, J. Park, and E.-H. Lee, "Numerical investigation of layered homogeneous skull model for simulations of transcranial focused ultrasound," *Neuromodulation: Technology at the Neural Interface*, vol. 28, no. 1, pp. 103-114, 2025.

[33] Q. Fang, and D. A. Boas, "Tetrahedral mesh generation from volumetric binary and grayscale images." pp. 1142-1145.

[34] S. Hang, "TetGen, a Delaunay-based quality tetrahedral mesh generator," *ACM Trans. Math. Softw*, vol. 41, no. 2, pp. 11, 2015.

[35] M. Köhler, and S. Goetz, "TMS coil design instrument (Kl/Codein Box): A toolbox for creating user-defined coils from conductor path data," *Brain Stimulation*, vol. 16, no. 3, pp. 698-700, 2023.

[36] O. Puonti, K. Van Leemput, G. B. Saturnino, H. R. Siebner, K. H. Madsen, and A. Thielscher, "Accurate and robust whole-head segmentation from

magnetic resonance images for individualized head modeling," *Neuroimage*, vol. 219, pp. 117044, 2020.

[37]N. M. Boayue, G. Csifcsák, O. Puonti, A. Thielscher, and M. Mittner, "Head models of healthy and depressed adults for simulating the electric fields of non-invasive electric brain stimulation," *F1000Research*, vol. 7, pp. 704, 2018.

[38]H. Song, W. Jung, E. Lee, J.-Y. Park, M. S. Kim, M.-C. Lee, and H.-I. Kim, "Capsular stroke modeling based on somatotopic mapping of motor fibers," *Journal of Cerebral Blood Flow & Metabolism*, vol. 37, no. 8, pp. 2928-2937, 2017.

[39]M. G. Christiansen, C. M. Howe, D. C. Bono, D. J. Perreault, and P. Anikeeva, "Practical methods for generating alternating magnetic fields for biomedical research," *Review of Scientific Instruments*, vol. 88, no. 8, 2017.

[40]J. Cho, S. Ryu, S. Lee, J. Kim, J.-Y. Park, H.-S. Kwon, and H.-I. Kim, "Clozapine-induced chemogenetic neuromodulation rescues post-stroke deficits after chronic capsular infarct," *Translational Stroke Research*, vol. 14, no. 4, pp. 499-512, 2023.

[41]H.-S. Kim, D. Kim, R. G. Kim, J.-M. Kim, E. Chung, P. R. Neto, M.-C. Lee, and H.-I. Kim, "A rat model of photothrombotic capsular infarct with a marked motor deficit: a behavioral, histologic, and microPET study," *Journal of Cerebral Blood Flow & Metabolism*, vol. 34, no. 4, pp. 683-689, 2014.

[42]A. Klein, L.-A. R. Sacrey, I. Q. Whishaw, and S. B. Dunnett, "The use of rodent skilled reaching as a translational model for investigating brain damage and disease," *Neuroscience & Biobehavioral Reviews*, vol. 36, no. 3, pp. 1030-1042, 2012.

[43]R. G. Kim, J. Cho, J. Ree, H.-S. Kim, P. Rosa-Neto, J.-M. Kim, M.-C. Lee, and H.-I. Kim, "Sensory-parietal cortical stimulation improves motor recovery in severe capsular infarct," *Journal of Cerebral Blood Flow & Metabolism*, vol. 36, no. 12, pp. 2211-2222, 2016.

[44]J. Cho, D.-H. Kwon, R. G. Kim, H. Song, P. Rosa-Neto, M.-C. Lee, and H.-I. Kim, "Remodeling of neuronal circuits after reach training in chronic capsular stroke," *Neurorehabilitation and Neural Repair*, vol. 30, no. 10, pp. 941-950, 2016.

[45]M.-H. Nam, J. Cho, D.-H. Kwon, J.-Y. Park, J. Woo, J. M. Lee, S. Lee, H. Y. Ko, W. Won, and R. G. Kim, "Excessive astrocytic GABA causes cortical hypometabolism and impedes functional recovery after subcortical stroke," *Cell reports*, vol. 32, no. 1, 2020.

[46]W. Sun, Q. Wu, L. Gao, Z. Zheng, H. Xiang, K. Yang, B. Yu, and J. Yao, "Advancements in transcranial magnetic stimulation research and the path to precision," *Neuropsychiatric Disease and Treatment*, pp. 1841-1851, 2023.

[47]H. Johansen-Berg, "Structural plasticity: rewiring the brain," *Current Biology*, vol. 17, no. 4, pp. R141-R144, 2007.

[48]C. Grefkes, and G. R. Fink, "Connectivity-based approaches in stroke and recovery of function," *The Lancet Neurology*, vol. 13, no. 2, pp. 206-216, 2014.

[49]J. Moretti, D. J. Terstege, E. Z. Poh, J. R. Epp, and J. Rodger, "Low intensity repetitive transcranial magnetic stimulation modulates brain-wide functional connectivity to promote anti-correlated c-Fos expression," *Scientific Reports*, vol. 12, no. 1, pp. 20571, 2022.

[50]P. d'Errico, I. Früholz, M. Meyer-Luehmann, and A. Vlachos, "Neuroprotective and plasticity promoting effects of repetitive transcranial magnetic stimulation (rTMS): a role for microglia," *Brain Stimulation*, 2025.

[51]F. Guo, J. Lou, X. Han, Y. Deng, and X. Huang, "Repetitive transcranial magnetic stimulation ameliorates cognitive impairment by enhancing neurogenesis and suppressing apoptosis in the hippocampus in rats with ischemic stroke," *Frontiers in physiology*, vol. 8, pp. 559, 2017.

[52]A. V. Peterchev, B. Luber, G. G. Westin, and S. H. Lisanby, "Pulse width affects scalp sensation of transcranial magnetic stimulation," *Brain stimulation*, vol. 10, no. 1, pp. 99-105, 2017.

[53]H. R. Siebner, K. Funke, A. S. Aberra, A. Antal, S. Bestmann, R. Chen, J. Classen, M. Davare, V. Di Lazzaro, and P. T. Fox, "Transcranial magnetic stimulation of the brain: What is stimulated?–A consensus and critical position paper," *Clinical neurophysiology*, vol. 140, pp. 59-97, 2022.

[54]K. Makowiecki, A. R. Harvey, R. M. Sherrard, and J. Rodger, "Low-intensity repetitive transcranial magnetic stimulation improves abnormal visual cortical circuit topography and upregulates BDNF in mice," *Journal of Neuroscience*, vol. 34, no. 32, pp. 10780-10792, 2014.

[55]C. S. Herrmann, S. Rach, T. Neuling, and D. Strüber, "Transcranial alternating current stimulation: a review of the underlying mechanisms and modulation of cognitive processes," *Frontiers in human neuroscience*, vol. 7, pp. 279, 2013.

[56]E. Trial, "Epidural Electrical Stimulation for Stroke Rehabilitation: Results of the Prospective, Multicenter, Randomized, Single-Blinded," 2015.

[57]M. Hallett, "Transcranial magnetic stimulation: a primer," *Neuron*, vol. 55, no. 2, pp. 187-199, 2007.

[58]V. V. Krylov, "Biological effects of weak magnetic fields: can the radical-pair mechanism provide a universal explanation?," *Biological Reviews*, 2025.

[59]H. Zadeh-Haghighi, and C. Simon, "Magnetic field effects in biology from the perspective of the radical pair mechanism," *Journal of the Royal Society Interface*, vol. 19, no. 193, pp. 20220325, 2022.

[60]A. D. Tang, W. Bennett, C. Hadrill, J. Collins, B. Fulopova, K. Wills, A. Bindoff, R. Puri, M. I. Garry, and M. R. Hinder, "Low intensity repetitive transcranial magnetic stimulation modulates skilled motor learning in adult mice," *Scientific reports*, vol. 8, no. 1, pp. 4016, 2018.

[61]J. Jaworski, K. Kalita, and E. Knapska, "c-Fos and neuronal plasticity: the aftermath of Kaczmarek's theory," *Acta neurobiologiae experimentalis*, vol. 78, no. 4, pp. 287-296, 2018.